Accepted Manuscript. Molecular and Cellular Neuroscience 2010, 44(4): 374-385. doi: 10.1016/j.mcn.2010.05.002

Developmental expression of Synaptotagmin isoforms in single calyx of Held-generating neurons

Running title: Synaptotagmin isoforms at the calyx of Held

Le Xiao[1], Yunyun Han[1], Heike Runne[2], Heather Murray[1], Olexiy Kochubey[1], Ruth Luthi-Carter[2] and Ralf Schneggenburger[1]

[1] Laboratory of Synaptic Mechanisms and [2] Laboratory of Functional Neurogenomics, Brain-Mind Institute, École Polytechnique Fédérale de Lausanne (EPFL), 1015 Lausanne, Switzerland

Correspondence:
Dr. Ralf Schneggenburger
Laboratory of Synaptic Mechanisms
École Polytechnique Fédérale de Lausanne (EPFL), Brain Mind Institute
1015 Lausanne, Switzerland
e-mail: ralf.schneggenburger@epfl.ch Tel. +41 21 693 5364 Fax +41 21 693 5350

5 Figures, 38 pages • 1 Suppl. Figure

Keywords: quantitative PCR, mRNA, gene expression profiling, presynaptic protein, auditory, bushy cell, Ca^{2+} sensor.

Abstract

The large glutamatergic calyx of Held synapse in the auditory brainstem has become a powerful model for studying transmitter release mechanisms, but the molecular bases of presynaptic function at this synapse are not well known. Here, we have used single-cell quantitative PCR (qPCR) to study the developmental expression of all major Synaptotagmin (Syt) isoforms in putative calyx of Held - generating neurons (globular bushy cells) of the ventral cochlear nucleus. Using electrophysiological criteria and the expression of marker genes including VGluTs (vesicular glutamate transporters), Ca^{2+} binding proteins, and the transcription factor Math5, we identified a subset of the recorded neurons as putative calyx of Held - generating bushy cells. At postnatal days 12 - 15 these neurons expressed Syt-2 and Syt-11, and also Syt-3, -4, -7 and -13 at lower levels, whereas Syt-1 and -9 were absent. Interestingly, early in development (at P3 - P6), immature bushy cells expressed a larger number of Syt-isoforms, with Syt-1, Syt-5, Syt-9 and Syt-13 detected in a significantly higher percentage of neurons. Our study sheds light on the molecular properties of putative calyx of Held - generating neurons and shows the developmental regulation of the Syt isoform expression profile in a single neuron type.

Introduction

The calyx of Held, a large glutamatergic synapse in the auditory brainstem circuit, has become a convenient model synapse to study transmitter release mechanisms in the CNS, because its large nerve terminal allows to perform direct presynaptic recordings (Forsythe, 1994; Borst et al., 1995; for review see Schneggenburger and Forsythe, 2006). The molecular bases of presynaptic function at the calyx of Held are, however, not well known. Knock-out studies in mice, which have examined synaptic transmission in forebrain neurons, have identified the function of presynaptic proteins in distinct steps of the presynaptic vesicle cycle (see Südhof, 2004 for a review). Many presynaptic proteins, however, exist in several isoforms, and these isoforms can be differentially expressed between forebrain and hindbrain regions (Kaeser et al., 2008; Ullrich et al., 1994). For this reason, a systematic evaluation of the expression of presynaptic proteins in the calyx of Held synapse would be highly desirable. More generally, expression profiles of genes with presynaptic functions have not been obtained for specific CNS neuron types.

The Synaptotagmin (Syt) gene family comprises about 15 members in mammals (Südhof, 2002; Craxton, 2001). Synaptotagmins contain two Ca^{2+}- and phospholipid - binding domains (the C2 domains), and Syt-1 and Syt-2 are known to play a critical role in fast Ca^{2+} triggered vesicle fusion at synapses (Geppert et al., 1994; Sun et al., 2007). In Syt-1 or Syt-2 k.o. animals, asynchronous transmitter release remains intact (Geppert et al., 1994; Sun et al., 2007), or is even enhanced relative to wild-type (Yoshihara and Littleton, 2002; Nishiki and Augustine, 2004). This has led to the view that a slower form of Ca^{2+}-triggered release must be mediated by a Ca^{2+} sensor distinct from Syt-1 and -2. Consequently, it has been proposed that other Syt isoforms might function as the Ca^{2+} sensor for slow release (Hui et al., 2005). At the calyx of Held, both a fast and a slow phase of release in response to prolonged Ca^{2+}

stimuli have been studied in detail (Sakaba and Neher, 2001; Wadel et al., 2007; Wölfel et al., 2007), and Syt-2 is critical for fast release (Sun et al., 2007). However, the putative Ca^{2+} sensor for slow release, as well as the expression profile of other Syt isoforms at the calyx of Held are unknown. Also, developmental changes in Ca^{2+} - secretion coupling around the onset of hearing (which occurs at ~ P12 in rodents; Blatchley et al., 1987) have been studied intensely at the calyx (Chuhma et al., 2001; Taschenberger et al., 2002; Fedchyshyn and Wang, 2005; Wang et al., 2008; Kochubey et al., 2009). However, developmental changes in the expression of presynaptic proteins that might drive these changes are unknown.

Here, we wished to determine the Syt-isoform expression profile at the calyx of Held, at developmental stages before, and after the onset of hearing in rats. We chose to perform the analysis on the level of mRNA detection, which should be amenable to high-throughput analysis, such as quantitative PCR (qPCR). Calyces of Held are formed by globular bushy cells in the ventral cochlear nucleus (VCN), which send their axons via the ventral acoustic stria to form calyces in the medial nucleus of the trapezoid body (MNTB) on the contralateral side (Harrison and Irving, 1966; Friauf and Ostwald, 1988; Spirou et al., 1990; Kuwabara et al., 1991; Smith et al., 1991). However, the VCN harbors various types of principal neurons (see Young and Oertel, 2004 for a review), and studying gene expression thus needs to take into account the heterogeneity of neuron types. Therefore, we have adopted techniques of single-cell RT- PCR (Lambolez et al., 1992; Monyer and Jonas, 1995; Toledo-Rodriguez et al., 2004; Durand et al., 2006), using a parallel qPCR approach which can detect up to 25 transcripts in a single cell. This has allowed us to analyze the expression of many Syt-isoform genes, as well as to include marker genes for glutamatergic - and GABAergic transmitter phenotype, Ca^{2+}-binding proteins and the transcription factor Math5 (Saul et al., 2008),

thereby facilitating the identification of putative calyx of Held - generating neurons in the VCN.

Results

Identification of putative calyx of Held-generating neurons by retrograde labeling

Previous lesion studies (Harrison and Irving, 1966) and single-axon recordings (Friauf and Ostwald, 1988; Spirou et al., 1990; Smith et al., 1991; Kuwabara et al., 1991) have shown that calyces of Held are formed by globular bushy cells in the VCN. In order to confirm these earlier findings with an independent technique, we used retrograde labeling techniques in which latex microbeads (Katz et al., 1984) were stereotactically injected into the MNTB of P13 rats. As shown in Fig. 1, the beads had labeled numerous neurons in the contralateral posterior VCN twelve days following injection (see Fig. 1A; yellow dots). The sections were double-stained with anti-CR and anti-PV antibodies, since we expected that calyx of Held-generating neurons should be PV- and CR- positive (Lohmann and Friauf, 1996; Felmy and Schneggenburger, 2004), as well as with the nuclear marker DAPI (Fig. 1B4; blue channel).

Closer inspection of bead-labeled neurons showed PV- and CR- positive neurons (Fig. 1B1, B2; red and green channel, respectively) that were surrounded by large nerve terminals (presumably representing auditory fiber input), which stained positive for either PV alone (see Fig. 1B4, arrow), or for both PV and CR (Fig. 1B4, arrowhead). Nerve fibers running in bundles nearby were also positive for PV alone, or for PV and CR (Fig. 1B4, star symbol). Since rat calyces of Held cells express PV, and, to a large degree also CR at P25 (Felmy and Schneggenburger, 2004), the retrogradely labeled cells found here most probably correspond to calyx of Held - generating neurons, or globular bushy cells (Pór et al., 2005). In the field of

view of Fig. 1B, two neurons were retrogradely labeled by beads (see Fig. 1B3 for the bead fluorescence channel).

To quantify the number of labeled neurons and their localization within the VCN, we counted the retrogradely labeled cells in each section, and plotted the cell count as a function of the section number along the anterior-posterior axis of the cochlear nucleus (Fig. 1C). In the more posterior region of the VCN many labeled neurons were apparent (Fig. 1C; section 5 - 20), whereas no labeled cells were found in the DCN, or in the most anterior part of the VCN. The position of labeled neurons relatively posterior in the VCN probably reflects the relatively posterior MNTB injection site in this animal (see Fig. 1C, lower bar). In total, in this experiment there were 307 labeled cells in the VCN contralateral to the injected MNTB, but only n = 12 cells in the VCN located *ipsilateral* to the injected MNTB (not shown). Two other injected rats also showed retrogradely labelled neurons in the contralateral VCN (n = 259 and 570 labelled cells), but a larger number of labelled cells was present in the *ipsilateral* VCN in these labeling experiments (n = 52 and 136), probably because the site of the injection was not limited to the MNTB (data not shown). Taken together, retrograde labeling confirms that calyx of Held-generating neurons are located in the contralateral VCN, and are largely represented by bushy cells which, at P25, express both PV and CR.

Electrophysiological identification of bushy cells and multipolar cells

We next used single-cell qPCR (see Experimental Methods) to detect the expression of 15 Syt-isoforms, as well as of several genes that might serve as markers of putative calyx of Held-generating neurons. We recorded from neurons with medium - to large soma size localized in transverse slices of the cochlear nucleus, excluding the most anterior- and the most posterior slice of the cochlear nucleus (see Experimental Methods). We used unlabeled

slices because we found that it was difficult to obtain whole-cell patch-clamp recordings of retrogradely labeled neurons with an acceptable success rate. To distinguish between bushy cells and multipolar cells which co-reside in this area of the VCN (Hackney et al., 1990), we recorded the intrinsic membrane properties of VCN neurons in current-clamp and voltage-clamp experiments. These experiments were first done at P12 - P15, shortly after the onset of hearing at ~ P12 in rats (Blatchley et al., 1987).

In current-clamp recordings, we observed two overall classes of firing properties. Fig. 2A shows an example of a bushy cell, which was distinguished by firing only a single action potential (AP) even in response to a strong depolarizing current injection. This cell had a fast membrane time constant (τ_m) of 1.1 ms (Fig. 2A, top), and the average value of τ_m was 3.7 ± 3.2 ms for all bushy cells at P12 - P15 (n = 105). In voltage-clamp, this cell showed a relatively small Na^+ current of about 5 nA, followed by fast and large voltage - dependent K^+ (outward) currents (Fig. 2A, bottom). In Fig. 2B, a multipolar cell is shown which fired several times with regular interspike intervals in response to depolarizing current injections, and had a relatively large Na^+ current amplitude (12.2 nA). In addition, the membrane time constant of this cell was slow (τ_m, 8.5 ms). The average value of τ_m was 17.3 ± 7.4 ms in all multipolar cells at P12 - P15; significantly slower than τ_m in bushy cells ($p < 10^{-4}$).

In a scatter plot of the number of APs as a function of the maximal Na^+ current amplitude (Fig. 2D), bushy cells tended to cluster at low numbers of APs and low apparent Na^+ current amplitude, whereas multipolar cells were preferentially localized at high numbers of APs and large Na^+ current amplitudes (Fig. 2D, open and filled data points, respectively). Neurons that were classified as bushy cells based on their firing properties had an average maximal Na^+ current amplitude of 5.1 ± 1.8 nA (n = 128 cells; mean ± S.D.), whereas multipolar cells had

maximal Na^+ currents of 11.0 ± 3.4 nA (n = 61 cells; mean ± S.D.); this difference was highly significant ($p < 10^{-4}$). Thus, the Na^+ current amplitude can be used as a further criterion to separate bushy cells from multipolar cells, in addition to the firing behaviour measured under current-clamp (Wu and Oertel, 1984; Lu et al., 2007).

We found that some bushy cells at P12 - P15 fired several APs at the onset of the depolarizing current injection (Fig. 2C; n = 35 out of 128 cells). Bushy cells with multiple AP firing were reported previously in young adult mice (Cao et al., 2007). These cells were also identified as bushy cells because firing was not maintained throughout the current pulse, and because later APs had smaller amplitudes (Fig. 2C). Finally, in Fig. 2E, a scatter plot of the number of APs versus Na^+ current amplitude is shown for putative bushy cells recorded at an earlier developmental stage, P3 - P6 (n = 29 cells). This data set will be described in more detail below.

Molecular characterization of multipolar and bushy cells by single-cell qPCR

We next analyzed the recorded bushy and multipolar cells in terms of their expressed gene transcripts using single-cell qPCR. We harvested the mRNA of single electrophysiologically characterized bushy- or multipolar cells from P12 - P15 old rats via the whole-cell recording pipette, followed by reverse transcription and qPCR analysis (see Experimental Methods). In addition to analyzing the expression of multiple Syt-isoforms, we also included a number of genes that serve as marker genes for glutamatergic neurons (vesicular glutamate transporters VGluT1, 2), GABAergic neurons (glutamate decarboxylases GAD65, GAD67; and vesicular GABA transporter, VGAT), as well as Ca^{2+} binding proteins and the transcription factors Math5 and MafB. A list of all 25 gene transcripts analyzed in most cells can be seen in Fig. 3C (left).

Figure 3A shows the results of the qPCR analysis of n = 11 selected gene transcripts out of a total of n = 25, for the same bushy cell as illustrated in Fig. 2A. The most strongly expressed genes crossed the threshold (0.2 fluorescence units; see dashed line in Fig. 3A) after ~ 22 - 24 cycles, including β-actin (Fig. 3A; black trace), VGluT1 (purple trace), PV (light grey trace), Syt-11 (dark blue trace) and Syt-2 (dark grey trace). A group of apparently less strongly expressed transcripts crossed the threshold after 27 - 31 cycles and included Math5 (Fig. 3A; red trace) and Syt-7 (ochre trace). Notably, Syt-1, Syt-3 and Syt-5 were not detected in this cell, since the corresponding fluorescence signals did not cross the threshold even after 40 cycles. In Fig. 3B, a qPCR plot for the same 11 transcripts is shown for a multipolar cell (same recording as illustrated in Fig. 2B). In this multipolar cell, Syt-1, Syt-7 and Math5 were not detected.

In order to visualize the expression pattern of all analyzed genes, we generated color-coded plots of the threshold - crossing cycle values of all cells processed in parallel for qPCR. In the resulting plot for one round of experiments (n = 12 cells plus several "slice controls"; Fig. 3C), dark colors represent strong expression (low CT value), and light colors represent the presence of lower levels of transcripts (high CT value), or the absence of detected transcript (cycle threshold > 40 cycles; white symbol). This plot therefore both shows the presence or absence of a detected gene transcript, but retains the quantitative information contained in analyzing the absolute CT value; the average absolute CT values for all detected gene transcripts are also plotted in Suppl. Fig. 1. In Fig. 3D, we plot the detection *frequency* for each gene irrespective of its absolute CT value, classifying the results as 'detected' or 'not detected' (n = 21 bushy cells and n = 11 multipolar cells from n = 3 independent rounds of

experiments). In this plot, a significant difference of detection percentage is indicated by a star-symbol ($p < 0.01$; Fisher's exact test).

We found that among the group of cell marker genes (Fig. 3C, top lanes), strongly expressed transcripts were PV, which was detected in all neurons, as well as VGluT1 (see also Fig. 3D). All cells except two in this sample set were also positive for VGluT2. The GABAergic neuron markers GAD65 and GAD67 were not detected, and the vesicular GABA transporter VGAT was absent in this sample of n = 12 cells (Fig. 3C), but was detected in a small fraction of cells (Fig. 3D; ~ 15 - 20%). Overall, despite the detection of VGAT in a minority of cells, the bushy cells and multipolar cells analyzed here showed clear expression of glutamatergic, and absence of most GABAergic marker genes.

With regard to the Ca^{2+} binding proteins, PV was detected in all bushy cells and CR was detected in approximately half of them, whereas CB was absent (Fig. 3C, D). CR was differentially expressed in the two cell types, with a significantly higher percentage of detection in bushy cells as compared to multipolar cells ($p < 0.05$; Fisher Exact test; see star symbol in Fig. 3D). This expression pattern of Ca^{2+} binding proteins is expected for calyx of Held - generating neurons, because calyces of Held express PV and, at P12 - P15, CR in a subset of all calyces (Felmy and Schneggenburger, 2004).

To further elucidate the molecular identity of calyx of Held generating neurons, we tested for the expression of the transcription factors Math5 and MafB in a subset of all investigated cells. Saul et al. (2008) have shown that Math5 is expressed very selectively in bushy cells of the mouse VCN, using transgenic mouse models. We detected Math5 transcript in five out of seven tested bushy cells, whereas Math5 was only detected in n = 1/5 multipolar cells (Fig.

3C, D). Due to the small sample number, this difference did not reach statistical significance ($p = 0.24$; Fisher's exact test). The transcription factor MafB, which is a marker for VCN neurons (Howell et al., 2007), was detected in all bushy cells analyzed here (n = 7/7), and in three out of five multipolar cells (Fig. 3C). Taken together, the expression of marker genes like VGluT1 and -2, and PV as well as Math5 confirms the bushy - cell identity of electrophysiolocigally characterized cells. The presence of CR transcripts in many of these bushy cells suggests that they are indeed putative calyx of Held - generating neurons (Felmy and Schneggenburger, 2004; Pór et al., 2005).

Synaptotagmin isoform expression in bushy cells and multipolar cells

Having convinced ourselves of the identity of the sampled bushy cell population, we next analyzed the expression of Syt-isoforms in bushy cells and multipolar cells recorded at P12 - P15 (Fig. 3C; lower lanes; Fig. 3D, *right*). The single-cell qPCR data shows that Syt-2 and Syt-11 are the two most widely and strongly expressed Syt-isoforms. These two isoforms were detected in a high percentage of both neuron types (~ 90%; Fig. 3D). Conversely, Syt-1, the isoform with the closest known functional homology to Syt-2 (Nagy et al., 2006; Xu et al., 2007), was not detected in bushy cells of P12 - P15 rats (Fig. 3A, C, D; n = 21 cells), whereas it was detected in about one-third of all the multipolar cells (Fig. 3C, D; $p < 0.05$). Syt-1 was the only Syt-isoform gene that was differentially expressed between bushy cells and multipolar cells (Fig. 3D; see star symbols).

Following Syt-2 and Syt-11, the next most widely-expressed Syt isoforms in both cell types were Syt-4, Syt-7, Syt-13 and Syt-3, which were found in 60 - 80% of all cells (for Syt-4, 7 and 13), or in 40 - 50% of all cells (for Syt-3), irrespective of neuron type (Fig. 3C, D). Syt isoforms that were not detected in either cell type were Syt-6, Syt-8 and Syt-9, whereas the

remaining isoforms (Syt-5, Syt-10 and Syt-12) were only found in a small percentage of neurons (~ 10 - 30%; Fig. 3D). These low detection rates could indicate that these isoforms are expressed in only a subset of cells. Alternatively, it remains possible that mRNAs at a low cytosolic concentration have sometimes escaped detection by single-cell qPCR. To address the question of the absolute transcript content and its variation between strongly- and weakly expressed genes, we plotted the average CT value for all transcripts detected in bushy cells of P12 - P15 rats (see Suppl. Fig. 1). This analysis showed that transcripts fell into roughly two groups: strongly expressed genes (with CT values ~ 25 - 26) and weakly expressed genes (with average CT values of 29 - 30).

Developmental regulation of Synaptotagmin isoform expression in bushy cells

To investigate a possible developmental regulation of the expression of various Syt isoforms in putative calyx of Held - generating neurons, we next investigated Syt-isoform expression at P3 - P6, which corresponds to a time shortly after the formation of the large calyces of Held at P2 - P4 (Hoffpauir et al., 2006; Rodriguez-Contreras et al., 2008). For this purpose, we now aimed at recording selectively from bushy cells. This was done by choosing cells with large, oval-shaped somata located close to the entry of the auditory fibers in the cochlear nucleus. Fig. 4A shows the firing properties and voltage-gated currents of an example cell. This cell fired several APs with decreasing amplitudes, and it had a slow membrane time constant (τ_m, 18.5 ms). On average, τ_m was 13.9 ± 6.1 ms (n = 29 cells), contrasting with the faster average value of 3.7 ms for bushy cells at P12 - P15 (see above; $p < 10^{-4}$). A scatter plot of the number of APs versus the measured Na^+ current amplitude was shown above (see Fig. 2E). The cells recorded at P3 - P6 responded with few action potentials at the onset of depolarizing current steps (1 - 4 APs; n = 17 out of 29 cells fired a single AP), and they had small Na^+ currents (3.2 ± 1.4 nA; see Fig. 2E). These cells therefore most likely represent immature bushy cells.

We used the expression of Math5 as a marker since this transcription factor was shown to be quite selectively expressed by bushy cells of the VCN (Saul et al., 2008). Among all cells recorded at P3 - P6 (n = 29), twenty-six were found to express Math5 by single-cell qPCR (see below). This confirms that most of the recorded cells at P3 - P6 were bushy cells, although it cannot be excluded at present that a small population of multipolar cells could also express Math5.

Fig. 4B shows the real-time PCR plot of the same neuron as illustrated in Fig. 4A. In this cell, we detected Syt-2 (dark grey trace) and Syt-5 (light blue trace) amongst other detected gene products, but PV (light grey trace) and Syt-1 (green trace) were not detected. All cells analyzed at P3 - P6 (n = 29) expressed VGluT1 and most expressed VGluT2, whereas GABAergic markers were absent (Fig. 4C, D), indicating that we recorded from glutamatergic neurons also at P3 - P6. The Ca^{2+} binding proteins PV and CR were detected in only a subset of neurons (Fig. 4C, D). This agrees with previous immunohistochemical findings showing a developmental expression onset of ~ P6 for PV, and ~ P10 for CR (Lohmann and Friauf, 1996; Felmy and Schneggenburger, 2004). The majority of cells expressed Math5 (n = 26/29). Thus, the expression profile of marker genes, especially the presence of Math5, suggests that we recorded from bushy cells (Saul et al., 2008).

In Fig. 4D, we compare the detection percentage of each gene in bushy cells at P3 - P6 (grey bar; n = 26 Math5-positive neurons out of a total of n = 29), with the one of bushy cells at P12 - P15 (open bars; re-plotted from Fig. 3D, open bars). The most apparent difference between the two developmental stages was the detection of a larger number of Syt-isoforms at the young age (Fig. 4D; compare also Figs 4C, and 3C). Thus, Syt-1, Syt-5, Syt-9 and Syt-13 were detected in a significantly higher percentage of neurons at P3 - P6, as compared to P12 -

P15 (see Fig. 4D, star symbols; $p < 0.05$; Fisher Exact test). On the other hand, Syt-12 was detected in a *smaller* percentage of cells at P3 - P6 compared to P12 - P15, consistent with the late expression onset of this Syt isoform (Maximov et al., 2007). Thus, the qPCR data suggests that Syt-1 and Syt-5, and, to a lesser degree also Syt-9, are expressed in a sizable fraction of immature bushy cells, and that these genes are downregulated during development (see Discussion).

Developmental localization of Syt1 and Syt2 in nerve terminals targeting the MNTB

Finally, we used immunohistochemistry with antibodies against Syt1, Syt2 and VGluT2 to investigate the presence of Syt1 and Syt2 proteins in glutamatergic nerve terminals that target the MNTB (Fig. 5). In double immunohistochemical stains of MNTB sections of a P14 rat, an anti-VGluT2 antibody revealed large calyces of Held that were also stained by the anti-Syt-2 antibody (Fig. 5A). The overlay image shows clear co-localization of both proteins in the large calyx of Held nerve terminals (Fig. 5A, *right*). In addition, there are numerous small bouton-like synapses positive for VGluT2 but not for Syt-2 (green bouton-like terminals in Fig. 5A *right*, arrow).

We next co-stained MNTB sections with antibodies against VGluT2 and Syt-1, to determine whether calyces of Held, or other synaptic terminals in the MNTB, contain Syt-1 (Fig. 5B). The anti-Syt-1 antibody stained terminals of relatively large size (~ 2 µm) located close to the somata of MNTB principal neurons, but most of these terminals were not co-stained by the VGluT2 antibody (see Fig. 5B arrow, for an example), suggesting that these are inhibitory terminals. In addition, the Syt-1 signal did not overlay with the calyceal nerve endings visualized by the VGluT2 immunoflourescence (Fig. 5B, right). These immunohistochemical data (Fig. 5A, B) show that calyces of Held of P12 - P15 rats contain Syt-2 but not Syt-1, in

agreement with our single-cell qPCR analysis in bushy cells (Fig. 3), and confirming previous results from immunohistochemistry in mice (Sun et al., 2007; Fox and Sanes, 2007).

Since we detected Syt-1 mRNA in a substantial fraction of bushy cells in P3 - P6 rats by single-cell qPCR (~ 50%; see above, Fig. 4), we investigated whether Syt-1 can be detected in young calyces of Held by immunohistochemistry. Fig. 5C shows co-staining with the anti-Syt-1 antibody and with the anti-VGluT2 antibody in a MNTB section from a P4 rat. The anti-VGluT2 antibody stains nascent calyces of Held, which at this young age are more irregular in morphology than at P14 (compare Fig. 5C with Fig. 5A, B; Rodriguez-Contreras et al., 2008). The VGluT2-positive large presynaptic structures at P4 co-stained with the Syt-2 antibody (not shown), indicating that young rat calyces contain Syt-2. However, no clear co-staining with the anti-Syt-1 antibody was observed (Fig. 5C). Interestingly, neighboring small synaptic boutons were stained by the anti-Syt-1 antibody either together with VGluT2, or in the absence of VGluT2 (Fig. 5C, right; arrow and arrowhead, respectively), suggesting that glutamatergic and non-glutamatergic bouton-like terminals contain Syt-1. Thus, Syt-1 is not present in young calyces of Held at P4, but it is present in a sub-population of small glutamatergic bouton-like terminals. However, the origin of these terminals is currently unknown (see Discussion).

Discussion

Although the calyx of Held synapse between calyceal afferents and MNTB principal neurons has been studied intensely with patch-clamp recordings (see Schneggenburger and Forsythe, 2006 for a review), little is known about the molecular identity of calyx of Held - generating neurons, or about the specific presynaptic protein complement of this large model synapse.

Here, we have used whole-cell recordings of neurons in the VCN combined with single-cell qPCR, as well as immunohistochemistry and retrograde labeling, to identify putative calyx of Held-generating neurons, and to study their developmental Synaptotagmin (Syt)-isoform expression profile.

The identity of calyx of Held - generating neurons

Early lesion studies (Harrison and Irving, 1966) and single-axon recordings of large-diameter trapezoid body axons (Friauf and Ostwald, 1988; Spirou et al., 1990; Smith et al., 1991; Kuwabara et al., 1991) have indicated that calyces of Held in the MNTB are formed by bushy cells located in the contralateral VCN, most likely representing the population of globular bushy cells (see Cant and Benson, 2003 for a review). Our results support this finding, since injection of a retrograde label into the MNTB stained PV- and CR- positive neurons with bushy-cell - like somata located in the contralateral VCN close to the entry of the auditory nerve (Fig. 1). Considering that the MNTB receives small, non-calyceal glutamatergic- as well as GABAergic / glycinergic inhibitory synapses in addition to the large calyces of Held (Hamann et al., 2003; Awatramani et al., 2005; see also Fig. 5), some of the labeled cells could also represent neurons that form small bouton-like synapses in the MNTB. However, it can be expected that the labeling efficiency is higher for neurons with large terminals since these likely take up retrograde label more readily. We observed that ~ 300 neurons in the contralateral VCN were labeled, whereas the rat MNTB contains an estimated number of ~ 4000 (Rodríguez-Contreras et al., 2006) or ~ 6000 (Kulecza et al., 2002) neurons. Because most MNTB principal cells receive only one calyx (Bergsman et al., 2004), and because only a minority of axons branch before making calyces (Rodríguez-Contreras et al., 2006), the number of calyx of Held - generating bushy cells in the VCN should be roughly equal or only slightly smaller than the number of MNTB principal cells. Thus, the number of retrogradely

labeled neurons corresponds to less than 10% of all calyx of Held - generating neurons, likely because the injection of retrograde label necessarily only filled part of the MNTB (Fig. 1C), and because not all terminals at the injection site might take up the retrograde label.

To analyze the expression of several cell marker genes and Syt isoforms in putative calyx of Held - generating neurons, we performed single-cell qPCR in whole-cell recorded neurons of VCN slices, and functionally identified bushy cells and their neighboring multipolar cells based on AP firing (Wu and Oertel, 1984; Lu et al., 2007) and Na^+ current amplitude (Fig. 2). Although we cannot measure the absolute Na^+ current faithfully due to space-clamp problems, the smaller apparent Na^+ current in bushy cells most likely indicates that there are fewer Na^+ channels in the soma-near compartment of bushy cells as compared to multipolar cells. Thus, analyzing the apparent Na^+ current amplitude can contribute to a separation of bushy cells and multipolar cells, although the mechanisms underlying this difference need to be established in future work. At the younger age studied here (P3 - P6), we did not attempt to identify neuron types by electrophysiological criteria since it is likely that the differential firing properties between bushy cells and multipolar cells is not yet apparent. However, the recorded neurons responded with few APs to depolarizing current steps, and the expression of Math5 in a large majority of the neurons recorded at P3 - P6 suggests that these cells were indeed immature bushy cells (Saul et al., 2008).

In a brain structure like the VCN, which consists of various neuron types with a paucity of neuron-type specific molecular markers (but see Saul et al., 2008), the method of single-cell qPCR to detect gene expression profiles could be advantageous over methods like *in situ* hybridization, since the latter method cannot easily distinguish between different cell types with similar soma morphology. We have shown here that 25 transcripts can be detected from

a single recorded cell (see also Toledo-Rodriguez et al., 2004), and it should be easily possible to extend the method to 30 transcripts or beyond. Thus, single-cell qPCR might prove useful to verify the expression of small groups of genes implicated in specific neuronal signalling pathways or in specific forms of pre- and postsynaptic plasticity, in neurons located in complex neuronal tissues.

Developmental expression profile of Synaptotagmin isoforms in calyx of Held-generating neurons

The single-cell qPCR analysis showed co-expression of various Syt isoforms in single bushy cells and multipolar cells, similar to single neurons in other brain areas (Kerr et al., 2008; Mittelsteadt et al., 2009). The Syt expression profile was suprisingly similar in bushy cells and multipolar cells at P12 - P15, with only Syt-1 expressed in a significantly higher fraction of multipolar cells as compared to bushy cells. In both neuron types, the most strongly expressed isoforms were Syt-2 and Syt-11, followed by Syt-3, Syt-4, Syt-7 and Syt-13. Interestingly, this Syt isoform expression profile is overall quite similar to the one found in hippocampal interneurons (Kerr et al., 2008) except for the predominance of Syt-2 and absence of Syt-1 in the auditory brainstem neurons studied here.

By performing single-cell qPCR analysis also in neurons from younger rats (P3 - P6), we studied the developmental changes of Syt isoform expression in a single identified neuron type. We found that at P3 - P6, bushy cells expressed more Syt isoforms than at P12 - P15, with Syt-1, Syt-5, Syt-9 and Syt-13 detected in a significantly higher percentage of cells than at P12 - P15 (Fig. 4D). Thus, young bushy cells have a richer Syt isoform expression complement than more mature bushy cells.

Using cultured neurons from Syt-1 k.o. mice, it has been shown that of all Syt-isoforms, only Syt-1, Syt-2 and Syt-9 can rescue fast transmitter release, suggesting that only these three isoforms can function as fast Ca^{2+} sensors (Xu et al., 2007; see also Stevens and Sullivan, 2003; Nagy et al., 2006 for Syt-2). We found that amongst these three Syt-isoforms, only Syt-2 is expressed in P12 - P15 bushy cells, whereas some P3 - P6 bushy cells also expressed Syt-1 and Syt-9. Immunohistochemically, however, Syt-1 was not detected at P14 nor at P4 in calyces of Held (Fig. 5), in keeping with earlier results in young mice (Sun et al., 2007). This might indicate that some bushy cells at P3 - P6 express Syt-1 as suggested by single-cell qPCR (Fig. 4C, D), but the protein level might be low and Syt-1 might not be targeted to calyces of Held. In general, our Syt-isoform expression data agree with recent findings from Syt-2 k.o. mice which showed the importance of Syt-2 for fast Ca^{2+} evoked transmitter release at the calyx of Held (Sun et al., 2007). Given our finding that bushy cells express a greater number of Syt-isoforms early in development, it might be interesting to investigate whether other Syt-isoforms can support Ca^{2+} - dependent release in the absence of Syt-2, particularly at young ages.

The most convincing developmentally regulated Syt isoform was Syt-5, which was detected at relatively high levels in nearly each bushy cells at P3 - P6, but which was absent from most bushy cells at P12 - P15 (Fig. 4). This suggests a selective role for Syt-5 early postnatally, at a time when calyces of Held form. The function of Syt-5 is not well investigated in brain, but Syt-5 is present on secretory granules of pancreatic cells and PC12 cells, and involved in Ca^{2+}-dependent secretion in neuroendocrine cells (Saegusa et al., 2002; Iezzi et al., 2004). Interestingly, a recent EM study has found evidence for dense core vesicles in developing calyces of Held (Hoffpauir et al., 2006). Therefore, it is possible that Syt-5 could be present on dense core transport vesicles which might have a role during synaptogenesis (Ahmari et

al., 2000; Shapira et al., 2003). It is also possible that some of the Syt-isoforms that were expressed more abundantly in young calyces (Syt-1, Syt-5, Syt-9) mediate asynchronous transmitter release observed in developing calyces of Held (Chuhma et al., 2001).

Amongst all Syt-isoforms detected here, four do not bind Ca^{2+} (Syt-4 and Syt-11; von Poser et al., 1997), Syt-12 (Hui et al., 2005; Maximov et al., 2007), and Syt-13 (von Poser and Südhof, 2001). This would leave Syt-3 and Syt-7, in addition to Syt-2 (and Syt-5 in young calyces), as Syt isoforms with a documented Ca^{2+}-binding. Syt-3 and Syt-7 are localized at the plasma membrane, but not in the vesicle membrane (Butz et al., 1999; Sugita et al., 2001), and a recent paper showed that Syt-7 is an essential Ca^{2+} sensor for a large part of both the fast and the slow secretory response in chromaffin cells (Schonn et al., 2008). Thus, it might be useful to investigate the role of these isoforms in Ca^{2+} - dependent presynaptic function at the calyx of Held synapse.

Experimental Methods

Slice preparation and electrophysiology

Transverse 180µm thick brainstem slices were made with a vibratome (Leica TV1000S, Germany) on the level of the ventral cochlear nucleus (VCN). Wistar rats of postnatal days P12 - P15, or of P3 - P6 were used, with P0 referring to the day of birth. During the dissection of the brain and the slicing procedure, special care was taken to preserve the cochlear nucleus region. The first posterior slice of the cochlear nucleus (containing mostly dorsal cochlear nucleus) and the last anterior slice of the cochlear nucleus (containing the most anterior part of the VCN) were discarded. With this procedure, we obtained two slices of the posterior and medial part of the VCN. These slices should contain globular bushy cells that generate calyces

of Held (area II of Harrison and Irving, 1966), and exclude the most anterior part of the VCN which mainly contains spherical bushy cells. Slices were kept at 37°C in a bicarbonate-buffered solution composed of the following (in mM): 125 NaCl, 25 $NaHCO_3$, 1.25 KCl, 2 $CaCl_2$, 1 $MgCl_2$, 25 glucose, 3 myo-inositol, 2 Na-pyruvate, 0.4 ascorbic acid, pH 7.4 when bubbled with 95% O_2 / 5% CO_2. During recordings, slices were perfused with the same solution at room temperature (21 - 23°C).

Whole-cell recordings were made on VCN neurons with soma size of ~ 20 µm, using an EPC-10 patch clamp amplifier (HEKA, Germany; controlled by "Patchmaster" software) in a set-up equipped with an upright microscope (Olympus, Japan) and infrared gradient contrast illumination (Luigs and Neumann, Ratingen, Germany). The pipette (intracellular) solution contained (in mM): 150 K-gluconate, 15 KCl, 10 HEPES, 0.5 $MgCl_2$, 5 NaCl, 0.2 EGTA; pH 7.2, 310 mOsm. We initially used patch pipettes with open-tip resistances of 2.5 - 4 MΩ, giving series resistances (R_s) of 4-8 MΩ. Later, and for all single-cell qPCR experiments, pipette resistances were 1.5 - 2 MΩ, giving R_s of 3-5 MΩ (compensation up to 90%). Data analysis was done with IgorPro 5.0 (Wavemetrics, Lake Oswego, OR). In current clamp, a spike was counted when the membrane potential (V_m) exceeded -20mV. The membrane time constant (τ) was analyzed by mono-exponential fits to the V_m trace in response to -100pA current injections (Fig. 2A-C). The input resistance (R_{in}) was calculated from current-clamp experiments using the V_m change measured at the end of a 100 ms current step, divided by the current step amplitude.

Single cell qPCR detection of gene transcripts

(1) Cytoplasm harvesting: Standard procedures were followed to guarantee RNAse-free conditions during patch-clamp recordings and mRNA-harvesting (Monyer and Jonas, 1995).

After establishing whole-cell recording of a VCN neuron, we briefly (~ 2 min) recorded under current- and voltage-clamp to characterize the intrinsic properties of the cell under study (Fig. 2). Subsequently, the cytoplasm of the recorded cell was aspirated into the recording pipette by applying gentle negative pressure for 3 min. Only cells that had a leak current < 200 pA and R_s < 5 MΩ during this procedure were processed further. Upon removing the pipette from the bath, the pipette tip was passed 2 - 3 times through the liquid-air interface, in an attempt to remove any debris attached to the outside of the patch pipette. The patch-pipette was mounted in a custom-made holding device, where its intracellular solution and cytoplasm contents were expelled into an Eppendorf tube containing 4µl H_2O and 1µl RNAse inhibitor (Promega, Dübendorf, Switzerland). During expulsion, we did not break the pipette tip, since we found that tip breaking increased non-specific background signals as determined by the "slice controls" described below. The harvested cytoplasm samples were frozen immediately at -80°C.

(2) Reverse transcription (RT): Samples from ~ 10 cells, a H_2O control, an intracellular solution control and additional slice controls (see below) were processed in parallel (see e.g. Fig. 3C). RT was done with the High-Capacity cDNA Reverse Transcription Kits (Applied Biosystems, Rotkreutz, Switzerland). The RT reaction was incubated at 25°C for 10 min, at 37°C for 120 min, and at 85°C for 5 sec. Subsequently, the products were frozen and stored at -20°C before further processing.

(3) Preamplification. The RT product was pre-amplified in a first multiplex PCR reaction with the primers for all gene transcripts to be detected, using the Taqman Pre-amplification Master Mix solution (Applied Biosystems). The Taqman assays for the rat gene transcripts were (all from Applied Biosystems): ß-actin (Rn00667869_m1), Calbindin (CB)

(Rn00583140_m1), Calretinin (CR) (= calbindin2, Rn00588816_m1), Parvalbumin (PV) (Rn00574541_m1), GAD65 (Rn00561244_m1), GAD67 (Rn00566593_m1), VGAT (Rn00824654_m1), VGluT1 (Rn00587830_m1), VGluT2 (Rn00584780_m1), Math5 (Rn02121924_s1), MafB (Rn00709456_s1), Syt1 (Rn01760470_m1), Syt3 (Rn00569396_m1), Syt4 (Rn01157571_m1), Syt5 (Rn00571136_m1), Syt6 (Rn00573432_m1), Syt7 (Rn00572234_m1), Syt8 (Rn00584120_m1), Syt9 (Rn00584114_m1), Syt10 (Rn01638371_m1), Syt11 (Rn00383057_m1), Syt12 (Rn00593706_m1), Syt13 (Rn00578161_m1), Syt15 (Rn00710814_m1). For Syt2, Applied Biosystems designed a separate assay against the untranslated region (forward primer: CCATCCCAGACTCCCTCTTGT; reverse primer: CCCAAAGCCCCACTCCT; reporter sequence: CAGTCATGGCTTCCCC), to avoid contamination from a Syt-2 expression vector handled in the lab at the same time. The PCR protocol for the preamplification reaction (total volume 50µl) was 95°C for 10 min, followed by 16 cycles of 15 sec at 95°C, and 4 min at 60°C.

(4) qPCR amplification: Following preamplification, a second real-time PCR was performed separately and in triplicate for each gene transcript, using the Taqman gene Universal PCR master mix. A Tecan pipetting robot (TECAN, Switzerland) was used to distribute the reaction reagents into a 384-well plate. Quantitative PCR (qPCR) was done in a 7900HT Fast Real-Time PCR System (Applied Biosystems), with temperature cycles of 95°C for 10 min initially, followed by 40 cycles at 95°C (15 sec each) and 60°C (1 min each). In the fluorescence reporter plot, the cycle threshold (CT) was defined in the exponential phase of the amplification curve, at a level of 0.2 fluorescence units (Fig. 2C).

(5) Validation of the qPCR- and preamplification efficiency. The efficiency of the qPCR reaction was validated using a dilution series of 8 ng to 0.25 ng of total RNA, prepared from a hindbrain mRNA extraction (RNeasy protect midi kit, Qiagen, USA). A plot of CT value versus the logarithm of the input amount of total RNA was fitted with a line to estimate the amplification efficiency of each probe. The mean amplification efficiency was 0.92 ± 0.022 (a value of 1 indicates ideal efficiency) and above 0.9 for all assays except for three which were between 0.8 and 0.9. The amplification efficiency of the qPCR reaction was also verified for material after pre-amplification, revealing a value of 0.91 ± 0.04, with individual assays showing a similar amplification efficiency to that observed for non-preamplified samples (see above).

(6) Controls: The following control experiments were performed during each round of sample processing, to exclude false-positive detection. *i*) a water control *ii*) intracellular solution was processed either alone, or after expulsion from a patch-pipette into the RT tube *iii*) A "patch-pipette slice control", designed to test for a possible contamination of the outside of the patch pipette with cell debris. For this control, a patch pipette filled with intracellular solution was placed into the slice at a position close to a previously recorded cell for 5-6 minutes (under slight positive pressure), and subsequently processed like a normal sample (see e.g. Fig. 3C and 4C; rightmost lanes).

(7) *Experimental series; and analysis and statistics of qPCR data*: n = 10 - 12 harvested cells, 4 - 5 slice controls, and 1 - 2 water controls were usually processed in parallel. The mRNA samples, which were stored at -80 °C, were thawed, reverse transcribed and pre-amplified (see above). The samples were distributed over three to five 384-well plates for qPCR analysis, in which a total of usually more than 1000 real-time PCR reactions were measured

(e.g. for the sample set in Fig. 3C: 25 genes x 16 samples x 3, since each real-time PCR was measured in triplicate = 1200). Each plot in Figure 3C and Figure 4C shows the results from one such round of samples processed in parallel. In these plots, each color-coded value is the average CT of real-time PCR in triplicate. If the cycle threshold was not crossed after 40 cycles, a gene was classified as "non-detected" (white color in Fig. 3C, D). In practice, all CT values of positive transcripts lay between 22 and 34 cycles, and the plots in Figs 3C and 4C are scaled accordingly. We then analyzed the percentage of cells in which a given gene was detected as "positive", for N = 21 bushy cells and N = 11 multipolar cells at P12 - P15 (Fig. 3D), and for N = 29 bushy cells at P3 - P6 (Fig. 4D, gray bars). To test whether the percentage of genes was significantly different between bushy cells and multipolar cells (at P12 - P15; see Fig. 3D), or between bushy cells at P3 - P6 and bushy cells at P12 - P15 (see Fig. 4D), we used the Fisher Exact test, with $p < 0.05$ as the limit for statistical significance (marked with a star-symbol in Figs 3D, 4D).

Retrograde labeling

Three P13 rats were stereotactically injected unilaterally into the MNTB with latex microspheres (Katz et al., 1984), using a single injection site aiming at the medial part of the MNTB in the anterior - posterior axis. We used a small volume (50 nl) of latex microspheres suspension with the aim to limit the injection to tissue within the MNTB. Injections were performed in a stereotactic frame (Model 940 Small Animal Stereotaxic Instrument, Kopf, USA) under anaesthesia conditions similarly as described by (Wimmer et al., 2004), in a procedure authorized by the Veterinary Authority of the Canton of Vaud, Switzerland (authorization number 1880). At P25, the rats were perfused transcardially with 4% PFA under pentobarbital anesthesia, and transverse sections of 40 µm were made through the entire cochlear nucleus complex. The injection site in the MNTB was inspected under the

fluorescence microscope. In two out of three injections, the bolus of the injection volume included part of the MNTB but also adjacent tissue; in one experiment (Fig. 1), the injection site was limited to within the MNTB. The sections were processed for immunohistochemistry with anti-PV and anti-CR antibodies (rabbit 1:5000, Swant, Switzerland, and mouse 1:500, Dako, Denmark, respectively), and the number of neurons containing retrograde label were counted in each section.

Immunohistochemistry

A P14 rat was transcardially perfused with 4% PFA under pentobarbital anaesthesia. The brain was post-fixed in 4% PFA for 24h, and dehydrated in 30% sucrose solution in PBS. Transverse brain sections of 30µm thickness on the level of the MNTB were made with a microtome (Leica, SM2400, Germany). The slices were processed similarly as previously described (Felmy and Schneggenburger, 2004), using the following primary antibodies: anti-VGluT2 (rabbit, Synaptic Systems 125403, 1:200), anti-Syt-2 (znp-1; mouse, ZIRC, Oregon, 1:200; see (Fox and Sanes, 2007), and anti-Syt1 (mouse, Synaptic Systems CL 41.1; 1:100). Secondary antibodies were: Alexa 488-conjugated anti-rabbit (Invitrogen A11008, 1:200), Alexa647-conjugated anti-mouse (Invitrogen A31571, 1:200). Confocal images were taken with a Leica SP2 Invert confocal microscope. For the P4 rat (Fig. 5B), transcardial perfusion was omitted.

Figure Legends.

Figure 1: **Retrograde labeling identifies putative calyx of Held - generating neurons in the ventral cochlear nucleus.** ***A***, A transverse brainstem section containing the posterior VCN and the dorsal cochlear nucleus contralateral to the injected MNTB. The dashed line marks the separation between VCN and dorsal cochlear nucleus. The retrogradely labeled neurons identified in this focal plane are identified by yellow dots. The box indicates the region shown in high-magnification images in ***B***. ***B1-B4***, High-magnification confocal images of the area indicated in ***A***, for three individual fluorescence channels (***B1***, CR immunofluorescence; ***B2***, PV immunofluorescence, ***B3*** fluorescence channel of the latex microbeads; ***B4***; overlay plus DAPI channel). Note the four PV- and CR-positive neurons with apposed somatic nerve endings that are either PV-positive (***B4***, arrow), or positive for both PV and CR (arrowhead). Scale bars are 200 and 20 µm in A, and B1 - B4 respectively. ***C***, Plot of the number of retrogradely labeled cells detected in each section, as a function of the position of the section along the anterior - posterior axis. The structures of the cochlear nucleus visible in each section are indicated below, as well as the extent of the MNTB and the site of the injection in the MNTB. The arrow identifies section number 10 that was shown in ***A***. AVCN: anterior VCN; PVCN: posterior VCN.

Figure 2: Separation of bushy cells and multipolar cells based on firing properties and Na^+ current amplitude. ***A*** **-** ***C*** Examples of current-clamp - (*upper* panels) and voltage-clamp recordings (*lower* panels), of a cell classified as bushy cell (***A***), as a multipolar cell (***B***), and as an 'atypical' bushy cell (**C**), all recorded in a age range of P12 - P15. Note the largely different firing properties of both cell types, the fast membrane time constant of the bushy cell in ***A***, as well as the smaller Na^+ current in both bushy cells (***A, C***) as compared with the multipolar cell (***B***). ***D***, Scatter plot of the number of APs for current injections of 500 pA, versus the maximal Na^+ current amplitude in each cell. Cells that were identified beforehand (based on their firing properties) as bushy cells (n = 128) and as multipolar cells (n = 61) are represented by open and filled symbols, respectively. Note the good separation between the two cell populations. ***E***, A similar plot as in D, for a population of cells investigated at P3 - P6 (see also Fig. 4 for the single-cell qPCR results from this group of immature cells).

Figure 3. Single-cell qPCR analysis of cell marker genes and Syt-isoforms in single electrophysiologically identified bushy cells and multipolar cells. ***A, B***, Examples of qPCR amplification plots for n = 11 transcripts for a bushy cell (***A***) and a multipolar cell (***B***). These cells are the same example cells as shown in Fig. 2A, B. Detected ("positive") genes crossed the threshold of 0.2 (see dotted line) after ~ 22 - 28 cycles, whereas non-detected genes did not cross the threshold even after 40 cycles. Note that the y-axis (reporter signal) is shown in linear scale for the bottom part, and in logarithmic scale for values above 0.01. ***C***, Color-coded plot of the absolute cycle threshold (CT) value for each gene, for n = 12 cells that were processed in parallel. Each row represents a gene, and each column represents a cell or control samples. The data are grouped to show (from left to right), bushy cells, multipolar cells, and slice controls (see Experimental Methods). Genes which were not detected (CT value > 40) are represented by a white symbol. The bushy cell and multipolar cell shown in **A** and ***B*** are shown here as cell 1 and as cell 10, respectively. ***D***, Plot of the expression frequency of each gene, plotted separately for bushy cells (open bars) and for multipolar cells (grey bars). Data from n = 21 bushy cells and n = 8 multipolar cells. Note that CR was detected in a significantly higher fraction of bushy cells, and that Syt-1 was detected in a significantly higher fraction of multipolar cells (star symbols indicate $p < 0.05$; Fisher's Exact Test). The data shown in this Figure was obtained from P12 - P15 old rats.

Figure 4: Single-cell qPCR analysis of gene expression in young bushy cells (P3 - P6). ***A***, Example of the firing properties (*upper* panel) and of the voltage-gated currents (*lower* panel) of a putative bushy cell of a P4 rat. ***B***, qPCR plot of n = 12 selected genes (out of a total of 25) analyzed in this cell. Note that this cell was positive for Math5 (see red lines) but negative for PV (light grey line). Same cell as illustrated in ***A***. ***C***, color-coded plot of the absolute cycle threshold (CT) value for each gene, for n = 11 cells that were processed in parallel, as well as for slice controls (right lanes; see Experimental Methods). Note that compared with the more mature bushy cells (Fig. 3C), most bushy cells were negative for PV and CR, but Math5 was detected in a majority of cells. Also note the strong presence of Syt-5 in most cells, which was essentially absent in more mature bushy cells (see Fig. 3C). ***D***, Plot of the expression frequency of each gene for a total of n = 29 bushy cells at P3 - P6. The data from more mature bushy cells (P12 - P15; open bars) is re-plotted from Fig. 3 D, to allow a direct comparison between the two age groups. Note that Syt-1, Syt-5, Syt-9 and Syt-13 was found in a significantly larger fraction of cells at P3 - P6 as compared to P12 - P15, whereas PV and Syt-12 were present in a significantly higher fraction in more mature bushy cells (star symbols indicates statistical significance; $p < 0.05$; Fisher's Exact Test).

Figure 5: Developmental expression of Syt-1 and Syt-2 in nerve terminals targeting the MNTB. In this Figure, immunohistochemistry with an anti-VGluT2 antibody (*left* panels), with anti-Syt-2 or anti-Syt-1 antibodies (*middle* panels; red channel), and the resulting overlay of the two immunofluorescence channels (*right* panels) are shown. ***A***, Co-staining with a polyclonal anti-VGluT2 antibody (*left* panel) and a monoclonal anti-Syt-2 antibody (znp-1, *middle* panel), in a P14 rat. Large calyces of Held are positive for both Syt-2 and for VGluT2. ***B***, Co-staining with the anti-VGluT2 antibody (*left* panel) and a monoclonal anti-Syt-1 antibody (CL41.1; *middle* panel), in a P14 rat. Note the absence of Syt-1 immunofluorescence in the large calyces of Held, while Syt-1 stains various VGluT2-positive and -negative terminals in the MNTB (see arrow for an example of a VGluT2-negative terminal). ***C***, Co-staining of a MNTB section from a P4 rat with the anti-VGluT2 antibody (*left* panel), and with the anti-Syt-1 antibody (*middle* panel). There was no detectable Syt-1 staining in the area of the nascent calyces of Held identified by VGluT2. The Syt-1 antibody stained small synaptic boutons that were either positive, or negative for VGluT2 (arrow, and arrowhead; respectively). This suggests that both at P4 and at P14 (B), Syt-1 is localized in some small glutamatergic and non-glutamatergic nerve terminals, but not in calyces of Held. Scale bar = 20 µm.

Acknowledgments: We thank Nicolas Michalski for comments on the manuscript. This work was supported by the Swiss National Science Foundation (3100A0-114069 to R.S.).

References:

Ahmari S.E., Buchanan J., Smith S.J., 2000. Assembly of presynaptic active zones from cytoplasmic transport packets. Nat Neuroscience 3, 445-451.

Awatramani G.B., Turecek R., Trussell L.O., 2005. Staggered development of GABAergic and glycinergic transmission in the MNTB. J Neurophysiol 93, 819-828.

Bergsman J.B., De Camilli P., McCormick D.A., 2004. Multiple large inputs to principal cells in the mouse medial nucleus of the trapezoid body. J Neurophysiol 92, 545-552.

Blatchley B.J., Cooper W.A., Coleman J.R., 1987. Development of auditory brainstem response to tone pip stimuli in the rat. Brain Res 429, 75-84.

Borst J.G.G., Helmchen F., Sakmann B., 1995. Pre- and postsynaptic whole-cell recordings in the medial nucleus of the trapezoid body of the rat. J Physiol 489, 825-840.

Butz S., Fernandez-Chacon R., Schmitz F., Jahn R., Sudhof T.C., 1999. The subcellular localizations of atypical synaptotagmins III and VI. Synaptotagmin III is enriched in synapses and synaptic plasma membranes but not in synaptic vesicles. J Biol Chem 274, 18290-18296.

Cant N.B., Benson C.G., 2003. Parallel auditory pathways: projection patterns of the different neuronal populations in the dorsal and ventral cochlear nuclei. Brain Res Bull 60, 457-474.

Cao X.J., Shatadal S., Oertel D., 2007. Voltage-sensitive conductances of bushy cells of the Mammalian ventral cochlear nucleus. J Neurophysiol 97, 3961-3975.

Chuhma N., Koyano K., Ohmori H., 2001. Synchronisation of neurotransmitter release during postnatal development in a calyceal presynaptic terminal of rat. J Physiol 530, 93-104.

Craxton M., 2001. Genomic analysis of synaptotagmin genes. Genomics 77, 43-49.

Durand G.M., Marandi N., Herberger S.D., Blum R., Konnerth A., 2006. Quantitative single-cell RT-PCR and Ca^{2+} imaging in brain slices. Pflugers Arch 451, 716-726.

Fedchyshyn M.J., Wang L.-Y., 2005. Developmental transformation of the release modality at the calyx of Held synapse. J Neuroscience 25, 4131-4140.

Felmy F., Schneggenburger R., 2004. Developmental expression of the Ca^{2+}-binding proteins calretinin and parvalbumin at the calyx of Held of rats and mice. Eur J Neurosci 20, 1473-1482.

Forsythe I.D., 1994. Direct patch recording from identified presynaptic terminals mediating glutamatergic EPSCs in the rat CNS, *in vitro*. J Physiol 479, 381-387.

Fox M.A., Sanes J.R., 2007. Synaptotagmin I and II are present in distinct subsets of central synapses. J Comp Neurology 503, 280-296.

Friauf E., Ostwald J., 1988. Divergent projections of physiologically characterized rat ventral cochlear nucleus neurons as shown by intra-axonal injection of horseradish peroxidase. Exp Brain Res 73, 263-284.

Geppert M., Goda Y., Hammer R.E., Li C., Rosahl T.W., Stevens C.F., Südhof T.C., 1994. Synaptotagmin I: A major Ca^{2+} sensor for transmitter release at a central synapse. Cell 79, 717-727.

Hackney C.M., Osen K.K., Kolston J., 1990. Anatomy of the cochlear nuclear complex of guinea pig. Anat Embryol 182, 123-149.

Hamann M., Billups B., Forsythe I.D., 2003. Non-calyceal excitatory inputs mediate low fidelity synaptic transmission in rat auditory brainstem slices. Eur J Neurosci 18, 2899-2902.

Harrison J.M., Irving R., 1966. Ascending connections of the anterior ventral cochlear nucleus in the rat. J Comp Neurol 126, 51-64.

Hoffpauir B.K., Grimes J.L., Mathers P.H., Spirou G.A., 2006. Synaptogenesis of the calyx of Held: Rapid onset of function and one-to-one morphological innervation. J Neuroscience 26, 5511-5523.

Howell D.M., Morgan W.J., Jarjour A.A., Spirou G.A., Berrebi A.S., Kennedy T.E., Mathers P.H., 2007. Molecular guidance cues necessary for axon pathfinding from the ventral cochlear nucleus. J Comp Neurol 504, 533-549.

Hui E., Bai J., Wang P., Sugimori M., Llinas R.R., Chapman E.R., 2005. Three distinct kinetics groupings of the synaptotagmin family: Candidate sensors for rapid and delayed exocytosis. Proc Natl Acad Sci U S A 102, 5210-5214.

Iezzi M., Kouri G., Fukuda M., Wollheim C.B., 2004. Synaptotagmin V and IX isoforms control Ca^{2+} -dependent insulin exocytosis. J Cell Sci 117, 3119-3127.

Kaeser P.S., Kwon H.B., Chiu C.Q., Deng L., Castillo P.E., Sudhof T.C., 2008. RIM1alpha and RIM1beta are synthesized from distinct promoters of the RIM1 gene to mediate differential but overlapping synaptic functions. J Neuroscience 28, 13435-13447.

Katz L.C., Burkhalter A., Dreyer W.J., 1984. Fluorescent latex microspheres as a retrograde neuronal marker for in vivo and in vitro studies of visual cortex. Nature 310, 498-500.

Kerr A.M., Reisinger E., Jonas P., 2008. Differential dependence of phasic transmitter release on synaptotagmin 1 at GABAergic and glutamatergic hippocampal synapses. Proc Natl Acad Sci U S A 105, 15581-15586.

Kochubey O., Han Y., Schneggenburger R., 2009. Developmental regulation of the intracellular Ca^{2+} sensitivity of vesicle fusion and Ca^{2+}-secretion coupling at the rat calyx of Held. J Physiol 587, 3009-3023.

Kulecza R.J.J., Vinuela A., Saldana E., Berrebi A.S., 2002. Unbiased stereological estimates of neuron number in subcortical auditory nuclei of the rat. Hear Res 168, 12-24.

Kuwabara N., DiCaprio R.A., Zook J.M., 1991. Afferents to the medial nucleus of the trapezoid body and their collateral projections. J Comp Neurol 314, 684-706.

Lambolez B., Audinat E., Bochet P., Crepel F., Rossier J., 1992. AMPA receptor subunits expressed by single Purkinje cells. Neuron 9, 247-258.

Lohmann C., Friauf E., 1996. Distribution of the calcium-binding proteins parvalbumin and calretinin in the auditory brainstem of adult and developing rats. J Comp Neurol 367, 90-109.

Lu Y., Harris J.A., Rubel E.W., 2007. Development of spontaneous miniature EPSCs in mouse AVCN neurons during a critical period of afferent-dependent neuron survival. J Neurophysiol 97, 635-646.

Maximov A., Shin O.H., Liu X., Sudhof T.C., 2007. Synaptotagmin-12, a synaptic vesicle phosphoprotein that modulates spontaneous neurotransmitter release. J Cell Biol 176, 113-124.

Mittelsteadt T., Seifert G., Alvarez-Baron E., Steinhauser C., Becker A.J., Schoch S., 2009. Differential mRNA expression patterns of the synaptotagmin gene family in the rodent brain. J Comp Neurol 512, 514-528.

Monyer H., Jonas P., 1995. Polymerase chain reaction analysis of ion channel expression in single neurons of brain slices. In: Single Channel Recording, ed Bert Sakmann, Erwin Neher 2nd ed., 1995, 357-373.

Nagy G., Kim J.H., Pang Z.P., Matti U., Rettig J., Sudhof T.C., Sorensen J.B., 2006. Different effects on fast exocytosis induced by synaptotagmin 1 and 2 isoforms and abundance but not by phosphorylation. J Neuroscience 26, 632-643.

Nishiki T., Augustine G., 2004. Synaptagmin I synchronizes transmitter release in mouse hippocampal neurons. J Neuroscience 24, 6127-6132.

Pór A., Pocsai K., Rusznák Z., Szücs G., 2005. Presence and distribution of three calcium binding proteins in projection neurons of the adult rat cohlear nucleus. Brain Res 1039, 63-74.

Rodriguez-Contreras A., van Hoeve J.S., Habets R.L., Locher H., Borst J.G., 2008. Dynamic development of the calyx of Held synapse. Proc Natl Acad Sci U S A 105, 5603-5608.

Rodríguez-Contreras A., de Lange R.P.J., Lucassen P.J., Borst J.G.G., 2006. Branching of calyceal afferents during postnatal development in the rat auditory brainstem. J Comp Neurol 496, 214-228.

Saegusa C., Fukuda M., Mikoshiba K., 2002. Synaptotagmin V is targeted to dense-core vesicles that undergo calcium-dependent exocytosis in PC12 cells. J Biol Chem 277, 24499-24505.

Sakaba T., Neher E., 2001. Calmodulin mediates rapid recruitment of fast-releasing synaptic vesicles at a calyx-type synapse. Neuron 32, 1119-1131.

Saul S.M., Brzezinski J.A., Altschuler R.A., Shore S.E., Rudolph D.D., Kabara L.L., Halsey K.E., Hufnagel R.B., Zhou J., Dolan D.F., Glaser T., 2008. Math5 expression and function in the central auditory system. Mol Cell Neurosci 37, 153-169.

Schneggenburger R., Forsythe I.D., 2006. The calyx of Held. Cell and Tissue Res 326, 311-337.

Schonn J.S., Maximov A., Lao Y., Sudhof T.C., Sorensen J.B., 2008. Synaptotagmin-1 and -7 are functionally overlapping Ca2+ sensors for exocytosis in adrenal chromaffin cells. Proc Natl Acad Sci U S A 105, 3998-4003.

Shapira M., Zhai A.G., Dresbach T., Bresler T., Torres V.I., Gundelfinger E.D., Ziv N.E., Garner C.C., 2003. Unitary assembly of presynaptic active zones from Piccolo-Bassoon transport vesicles. Neuron 38, 237-252.

Smith P.H., Joris P.X., Carney L.H., Yin T.C.T., 1991. Projections of physiologically characterized globular bushy cell axons from the cochlear nucleus of the cat. J Comp Neurol 304, 387-407.

Spirou G.A., Brownell W.E., Zidnac M., 1990. Recordings from cat trapezoid body and HRP labeling of globular bushy cell axons. J Neurophysiol 63, 1169-1190.

Stevens C.F., Sullivan J.M., 2003. The synaptotagmin C2A domain is part of the calcium sensor controlling fast synaptic transmission. Neuron 39, 299-308.

Südhof T.C., 2002. Synaptotagmins: Why so many? J Biol Chem 277, 7629-7632.

Südhof T.C., 2004. The synaptic vesicle cycle. Ann Rev Neurosci 27, 509-547.

Sugita S., Han W., Butz s., Liu X., Fernandez-Chacon R., Lao Y., Südhof T.C., 2001. Synaptotagmin VII as a plasma membrane Ca^{2+} sensor in exocytosis. Neuron 30, 459-473.

Sun J., Pang Z.P., Qin D., Fahim A.T., Adachi R., Sudhof T.C., 2007. A dual-Ca^{2+}-sensor model for neurotransmitter release in a central synapse. Nature 450, 676-682.

Taschenberger H., Leao R.M., Rowland K.C., Spirou G.A., v. Gersdorff H., 2002. Optimizing synaptic architecture and efficiency for high-frequency transmission. Neuron 36, 1127-1143.

Toledo-Rodriguez M., Blumenfeld B., Wu C., Luo J., Attali B., Goodman P., Markram H., 2004. Correlation maps allow neuronal electrical properties to be predicted from single-cell gene expression profiles in rat neocortex. Cereb Cortex 14, 1310-1327.

Ullrich B., Li C., Zhang J.Z., McMahon H., Anderson R.G.W., Geppert M., Südhof T.C., 1994. Functional properties of multiple synaptotagmins in brain. Neuron 13, 1281-1291.

von Poser C., Sudhof T.C., 2001. Synaptotagmin 13: structure and expression of a novel synaptotagmin. Eur J Cell Biol 80, 41-47.

von Poser C., Ichtchenko K., Shao X., Rizo J., Südhof T.C., 1997. The evolutionary pressure to inactivate. A subclass of Synaptotagmins with an amino acid substitution that abolishes Ca^{2+} binding. J Biol Chem 272, 14314-14319.

Wadel C., Neher E., Sakaba T., 2007. The coupling between synaptic vesicles and Ca^{2+} channels determines fast neurotransmitter release. Neuron 53, 563-575.

Wang L.-Y., Neher E., Taschenberger H., 2008. Synaptic vesicles in mature calyx of Held synapses sense higher nanodomain Calcium concentrations during action potential-evoked glutamate release. J Neuroscience 28, 14450-14458.

Wimmer V.C., Nevian T., Kuner T., 2004. Targeted in vivo expression of proteins in the calyx of Held. Pflugers Arch 449, 319-333.

Wölfel M., Lou X., Schneggenburger R., 2007. A mechanism intrinsic to the vesicle fusion machinery determines fast and slow transmitter release at a large CNS synapse. J Neuroscience 27, 3198-3210.

Wu S.H., Oertel D., 1984. Intracellular injection with horseradish peroxidase of physiologically characterized stellate and bushy cells in slices of mouse anteroventral cochlear nucleus. J Neuroscience 4, 1577-1588.

Xu J., Mashimo T., Südhof T.C., 2007. Synaptotagmin-1, -2, and -9: Ca^{2+} sensors for fast release that specify distinct presynaptic properties in subsets of neurons. Neuron 54, 567-581.

Yoshihara M., Littleton T., 2002. Synaptotagmin I functions as a Calcium sensor to synchronize neurotransmitter release. Neuron 36, 897-908.

Young E.D., Oertel D., 2004. Cochlear nucleus. In: The synaptic organization of the brain ed. by Gordon M. Shepherd.

Accepted Manuscript. Molecular and Cellular Neuroscience 2010, 44(4): 374-385. doi: 10.1016/j.mcn.2010.05.002

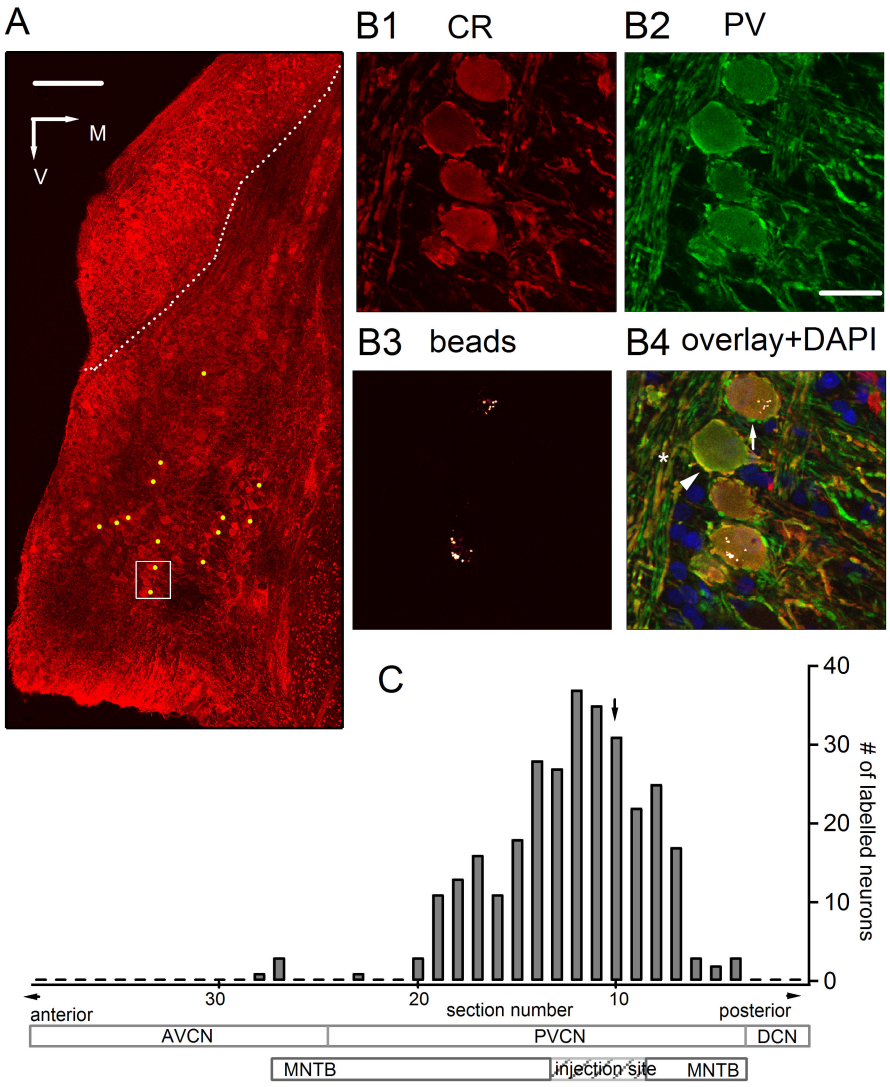

Figure 1

Accepted Manuscript. Molecular and Cellular Neuroscience 2010, 44(4): 374-385. doi: 10.1016/j.mcn.2010.05.002

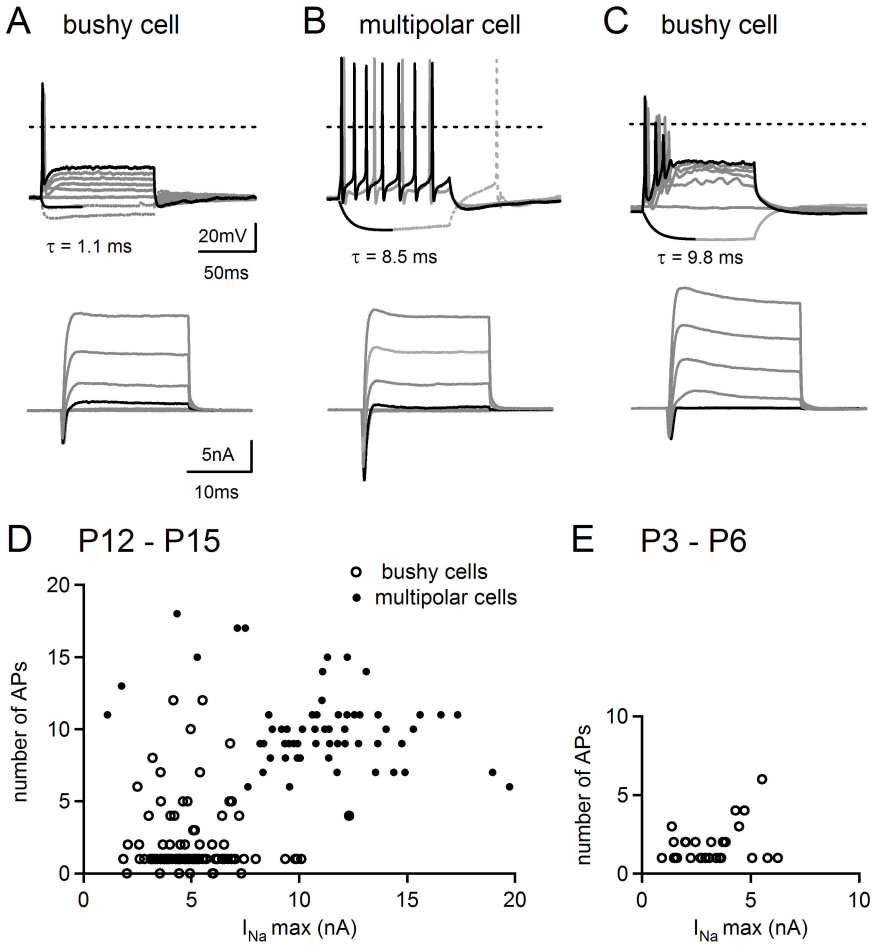

Figure 2

Accepted Manuscript. Molecular and Cellular Neuroscience 2010, 44(4): 374-385. doi: 10.1016/j.mcn.2010.05.002

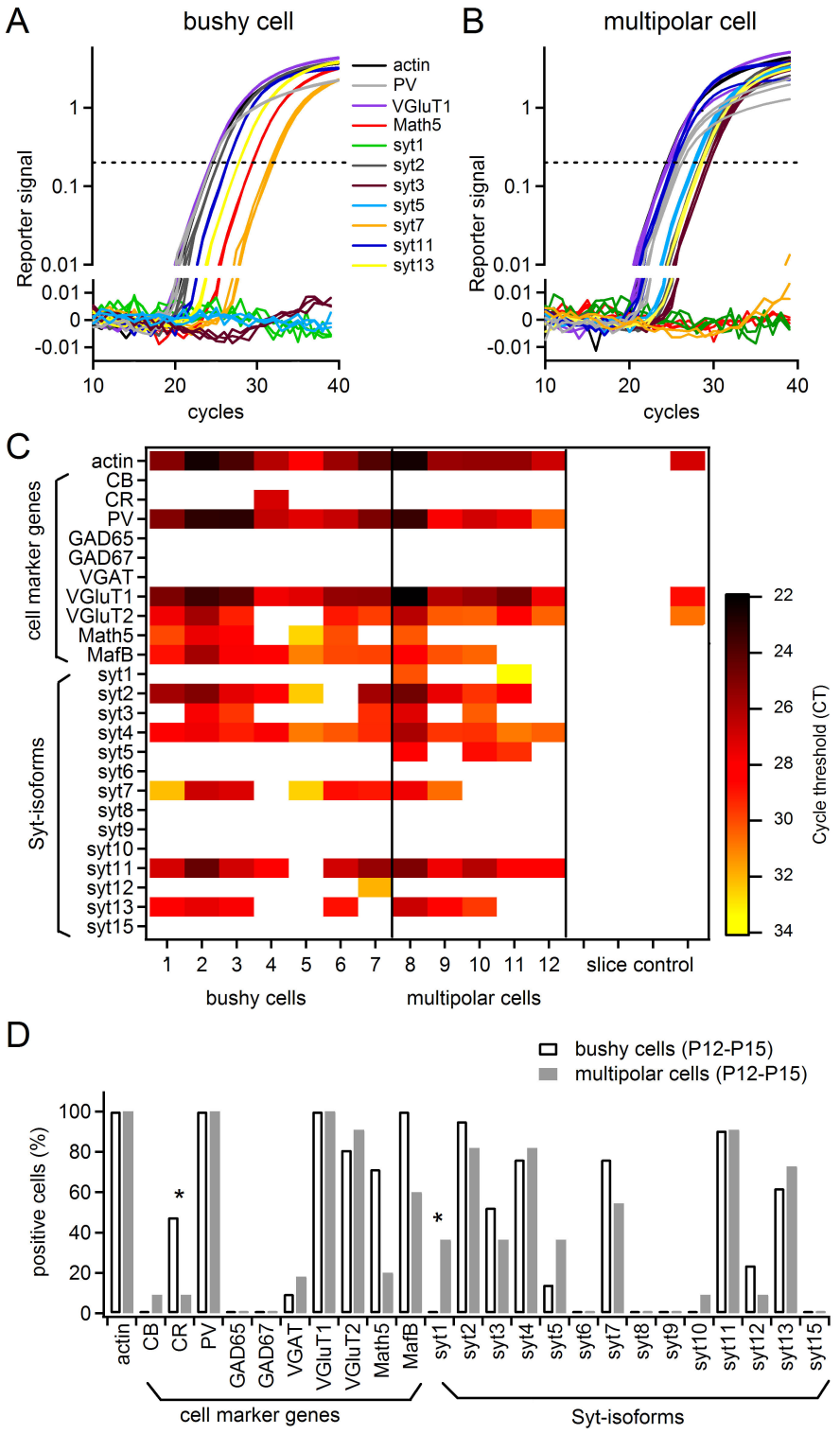

Figure 3

Accepted Manuscript. Molecular and Cellular Neuroscience 2010, 44(4): 374-385. doi: 10.1016/j.mcn.2010.05.002

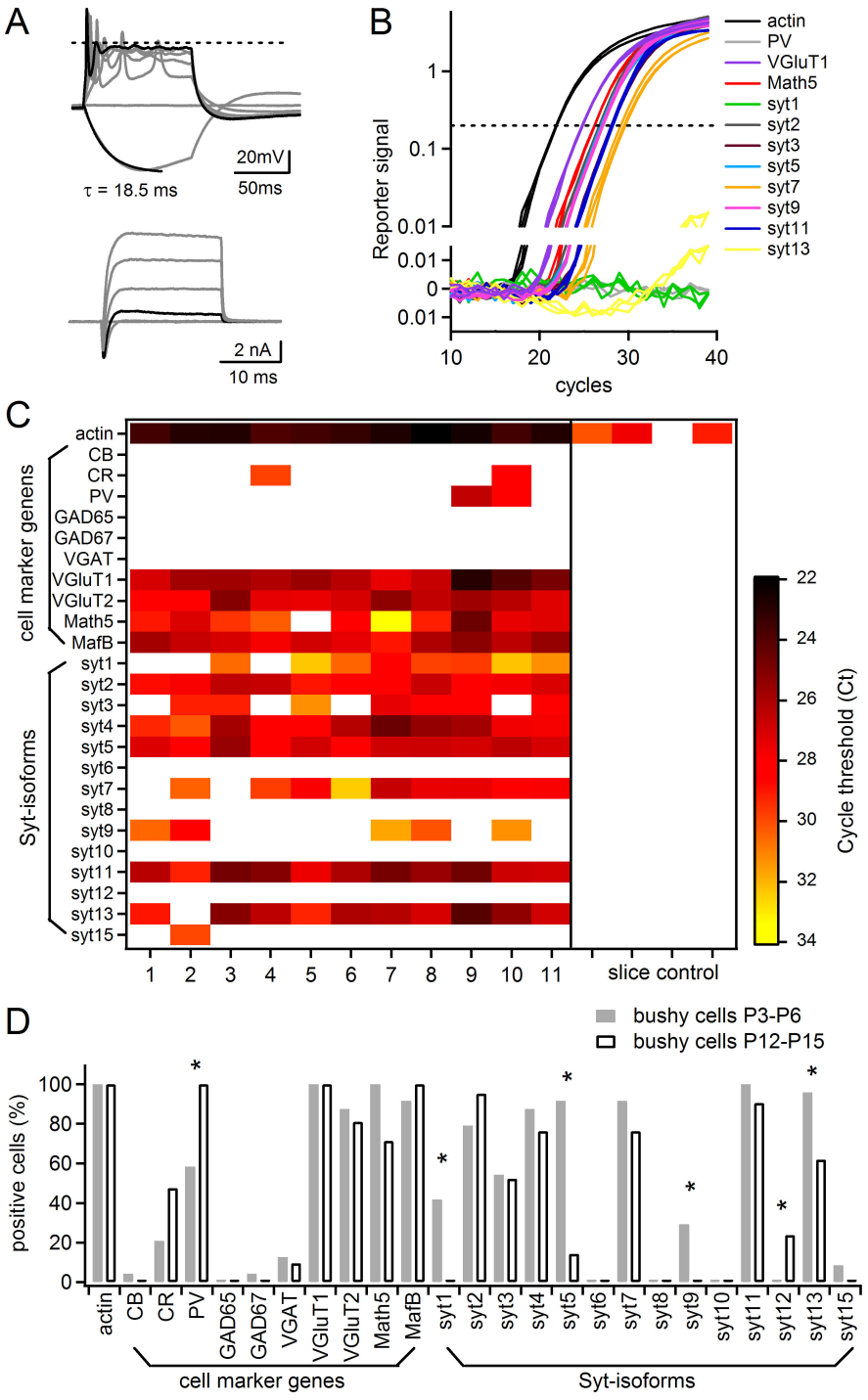

Figure 4

Accepted Manuscript. Molecular and Cellular Neuroscience 2010, 44(4): 374-385. doi: 10.1016/j.mcn.2010.05.002

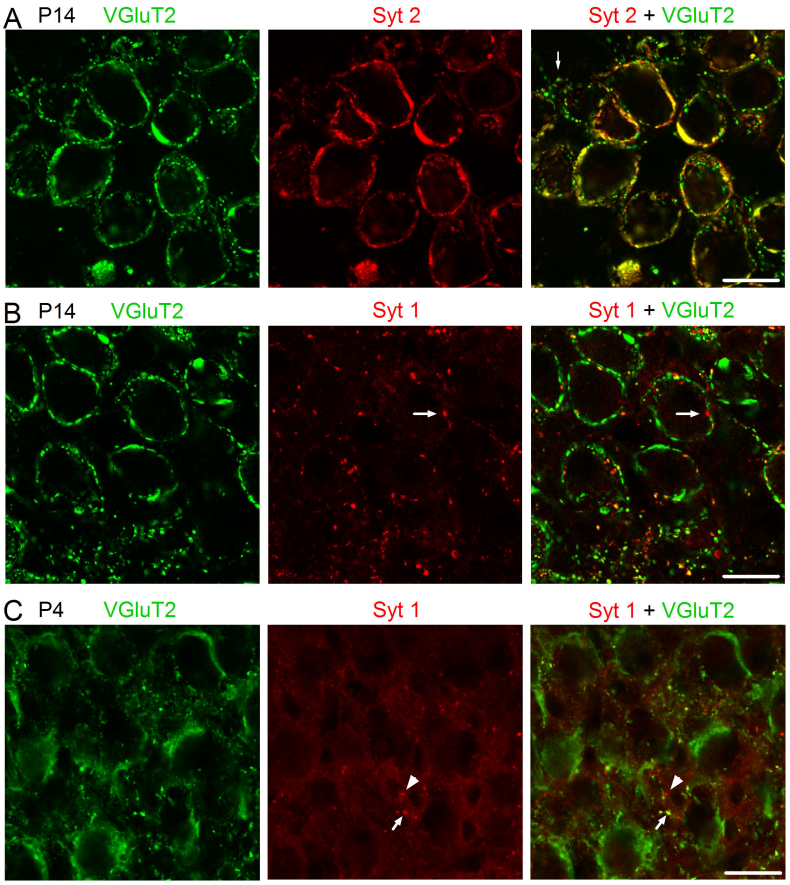

Figure 5